Contributions of interfaces on the mechanical behavior of 3D printed continuous fiber reinforced composites

Shixian Li, Kui Wang, Wanying Zhu, Said Ahzi, Francisco Chinesta

Contributions of interfaces on the mechanical behavior of 3D printed continuous fiber reinforced composites

Shixian Li [a,b], Kui Wang [a,*], Wanying Zhu [a], Yong Peng [a], Said Ahzi [b], Francisco Chinesta [c]

[a] Key Laboratory of Traffic Safety on Track of Ministry of Education, School of Traffic & Transportation Engineering, Central South University, Changsha 410075, China
[b] ICUBE Laboratory – CNRS, University of Strasbourg, Strasbourg 67000, France
[c] ESI Chair, PIMM, Arts et Métiers Institute of Technology, 151 Boulevard de l'Hopital, F-75013 Paris, France

Keywords:
3D printing
Continuous fiber
Stacking sequence
Stiffness model
Interfacial properties

A B S T R A C T

3D printing using continuous fiber reinforcement provides a new technical method for preparing complex components with high mechanical behaviors. However, these printed composites have great differences in interfacial behaviors, affecting overall performance. This study aimed to investigate the tensile behaviors of 3D printed continuous fiber filled composites. The structural evolutions and failure features of the composites induced by strain were analyzed with the consideration of interfaces, influenced by the reinforcement fibers, stacking sequences as well as raster orientations. A roller peeling test was conducted to quantify the interfacial strength of different materials. An analytical approach was proposed to predict the stiffness behavior of the printed composites by introducing an interfacial strengthening coefficient into the volume average stiffness model. The predictions of stiffness, for the 3D printed continuous fiber filled composites with different fibers, stacking sequences and raster orientations, were in good agreement with experimental results.

1. Introduction

Additive Manufacturing (AM), also known as 3D printing, is one of the most promising techniques for fabricating objects with complex structures and a relatively new way of providing customized products [1–3]. AM technologies encompass numerous methods, fused deposition method (FDM) is one of the most common AM approaches applied in commercial 3D printers due to its low cost, simple operation, low material waste and environmental friendliness [4,5]. For the same reason, FDM-AM is now being extended to industrial design and building applications [6]. Despite numerous printing polymers available, the relatively poor mechanical properties of pristine thermoplastic objects produced by FDM obstruct their application for structural purposes in various fields compared to traditional composites [7–9]. In recent years, reinforced fillers, such as continuous fibers, are widely used in FDM to improve the mechanical behaviors of 3D printed thermoplastic-based composites.

In literature, Van Der Klift et al. [10], Heidari-Rarani et al. [11], Dickson et al. [12] and Brooks et al. [13] found that continuous fiber reinforcement significantly increased the mechanical performances of 3D printed composites. Meanwhile, the mechanical properties of 3D printed continuous fiber reinforced composites highly depend on the printing parameters [14–19]. Peng et al. [15] evaluated the effect of printing orientations and stacking sequence (separated or concentrated sequence) on mechanical behaviors of continuous carbon fiber and short carbon fibers synergistically reinforced composites manufactured by 3D printing. They found that the introduction of $\pm 45^{\circ}$ layers into laminates significantly increased the energy absorption capability of composites. The mechanical properties of the composites were higher when the stacked continuous carbon fiber reinforced layers were separated in composites. This phenomenon was attributed to the much stronger adhesion of initial interfaces for the separated specimens than the concentrated ones. Yavas et al. [16] investigated the influence of staking sequences of the continuous and short carbon fiber reinforced composites layers on interlaminar shear strength. They discovered that the interfacial bonding strength between the printed layers of 3D printed composites played an important role in mechanical properties.

Meanwhile, researchers tried to use the classical laminated theory to predict the mechanical behaviors of 3D printed composites [20–22]. Unlike traditional manufacturing methods (formative or subtractive manufacturing), FDM approach allows a layer-by-layer build-up of components by depositing thin lines through nozzles [23,24]. In addition, FDM approach does not provide much pressure on the printing process [25,26]. Therefore, the continuous fibers reinforced composites

* Corresponding author.
E-mail addresses: kui.wang@csu.edu.cn, kui.wang@csu.edu.cn (K. Wang).

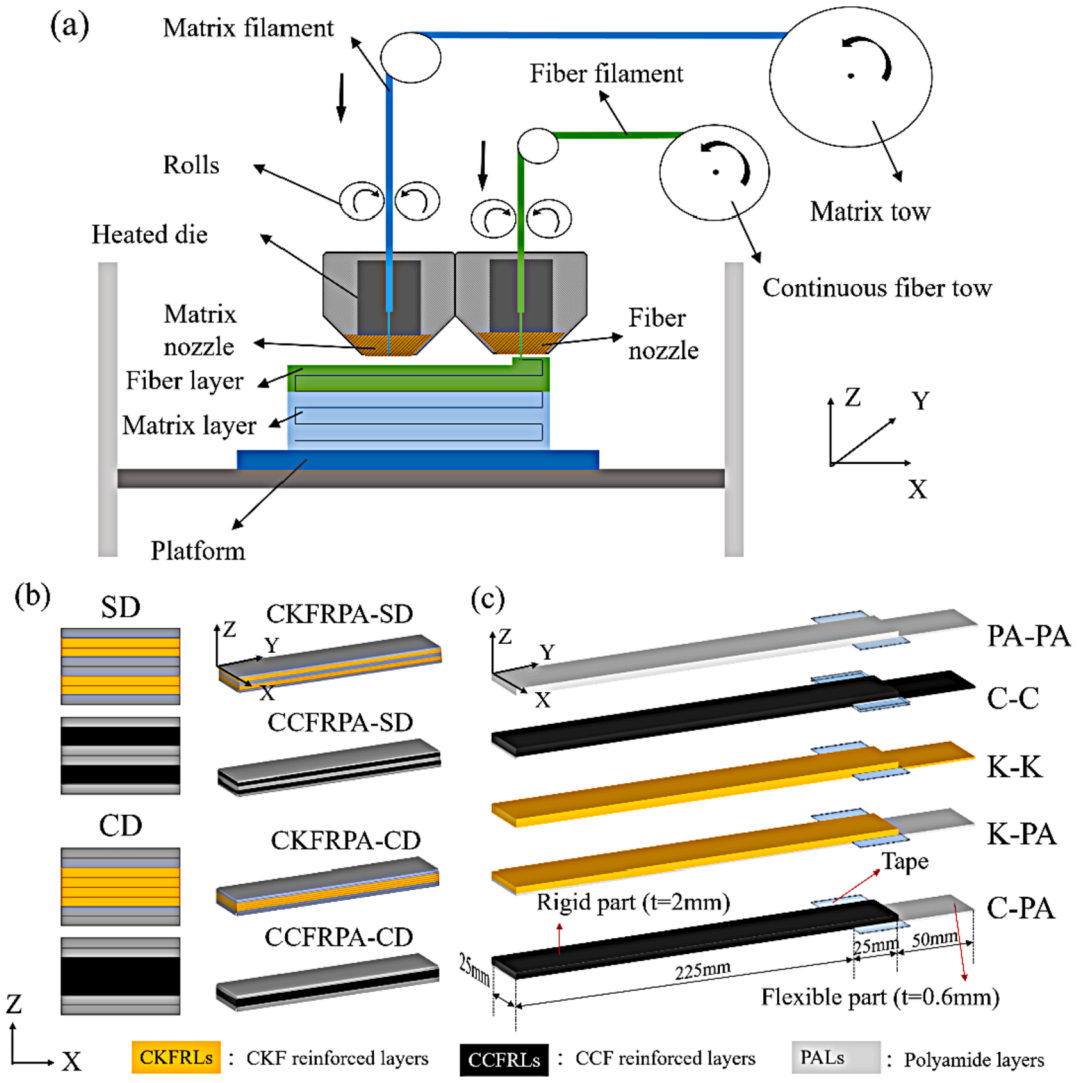

Fig. 1. Schematic presentation of (a) FDM process, 3D printed continuous fibers reinforced composites with (b) different stacking sequences and (c) peeling tests specimens with different interfaces.

prepared by 3D printed have great differences in interfacial properties between adjacent layers compared with those manufactured by traditional processes [27]. Moreover, in 3D printed multi-materials systems, the interface influences would be more important due to the different properties of interfaces between different materials and the different numbers of interfaces induced by the stacking sequence. In conclusion, it is essential to investigate the interlayer performance and to develop a prediction model considering different interface contributions for 3D printed continuous fiber filled composites.

In this study, continuous carbon fiber and continuous Kevlar fibers were used as reinforcements to prepare continuous fiber reinforced composites. The mechanical and interfacial behaviors of printed composites were studied by tensile and peeling tests, respectively. The structural evolutions induced by the strain of composites were captured at multi-scales to reveal the deformation and failure mechanisms with the effects of reinforcement fibers, stacking sequences and raster orientations. A prediction model considering interface contributions was established to predict the tensile modulus of composites.

2. Experimental methodologies

2.1. Materials and processing

In this study, polyamide (PA) filaments (1.75 mm, density of 1.1 g/cm3), continuous carbon fiber (CCF) filaments (0.38 mm, density of 1.4 g/cm3) and continuous Kevlar fiber (CKF) filaments (0.32 mm, density of 1.2 g/cm3) supplying from Markforged® were chosen as the thermoplastic matrix and reinforcements materials, respectively. Note that CCF and CKF filaments were not the group of pure continuous fibers. The reinforced continuous fiber filaments were composed of continuous carbon or Kevlar fiber bundles infused with a large amount of thermoplastic PA sizing agent [28]. Specifically, after thermogravimetric analysis, it was found that the CCF and CKF in filaments corresponded to 47.98 wt% and 40.85 wt%, respectively [29,38]. Prior to use, the materials were stored in a dry box to minimize the environment humidity.

A MarkForged® Mark7 3D printing equipment (Markforged, Cambridge, MA, USA) for the manufacturing process of continuous fiber reinforced composites was adopted in this study. The printer included two extrusion heads, allowing the printing of thermoplastic matrix and continuous fibers filaments independently (see Fig. 1(a)). Detailed information about this printing process can be found in our previous study [29]. The extrusion temperatures of the continuous fiber filaments and

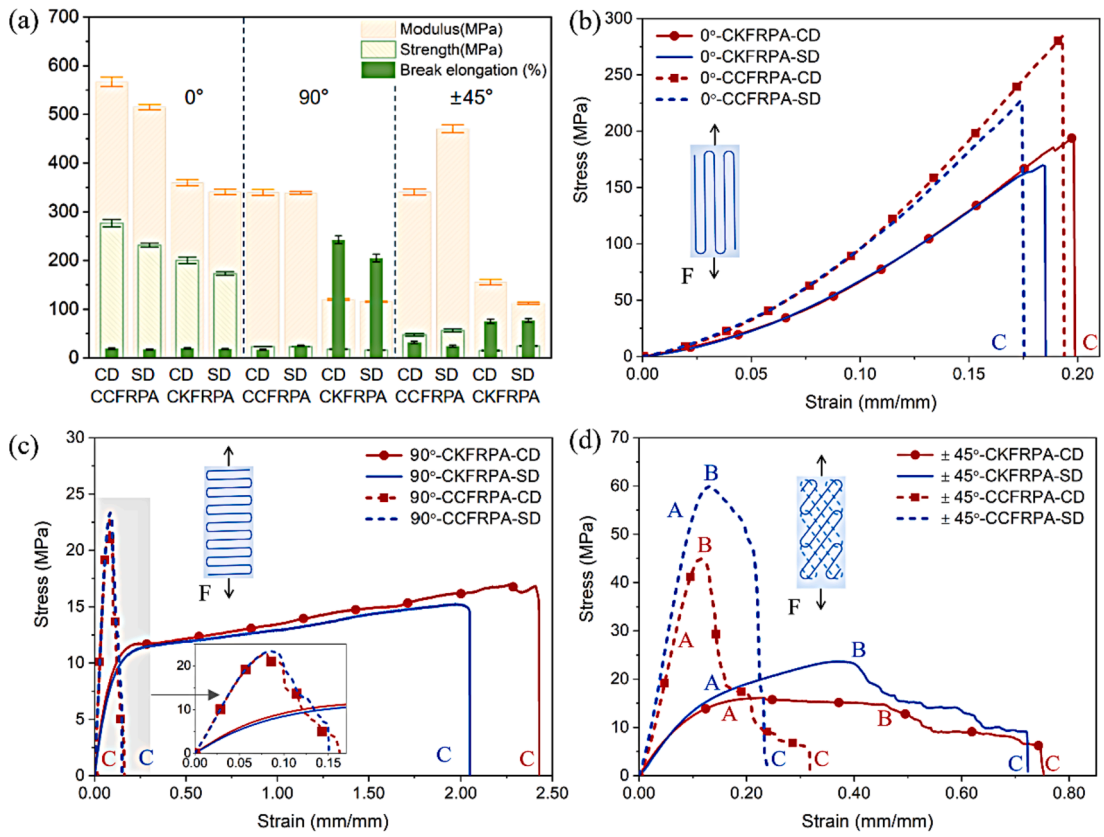

Fig. 2. Effects of fiber reinforcements, raster orientations and stacking sequences on (a) tensile modulus, tensile strength and elongation at break, and (b-d) tensile strain–stress curves of 3D printed continuous fiber reinforced composites.

matrix filaments were 270 °C and 255 °C, respectively.

2.2. Specimen preparation

2.2.1. Specimen for tensile test

Different from the traditional necked dog-bone shaped specimens for tensile testing, the geometrical shape of 3D printed continuous fiber reinforced composites should be determined carefully to ensure that the fibers are perfectly aligned without discontinuity [14]. Therefore, rectangular specimens were selected according to the ASTM D3039 standard. As shown in Fig. 1 (c), the tensile test specimens with the dimension of 80.0 mm × 5.0 mm × 1.0 mm were printed with different raster orientations (0°, ±45° or 90°) and stacking sequences (concentrated or separated distribution) of continuous fiber (see Fig. 1 (b)). Note that the 0° continuous fiber raster direction coincided with the X-axis, and the 90° continuous fiber raster direction coincided with the Y-axis.

In the following denotation, the printed composites with concentrated distribution (CD) and separated distribution (SD) of continuous carbon fiber reinforced layers (CCFRLs) or continuous Kevlar fiber reinforced layers (CKFRLs) were defined as CD and SD specimens, respectively. For example, the specimens with 0° continuous carbon fiber raster direction and separated distribution of CCFRLs were named 0°-CCFRPA-SD. The rest of the specimens could be named in the same way. All the specimens had a fixed layer number of a total of eight, including four continuous fiber layers (CKFRLs or CCFRLs), and four PA matrix layers (PALs). The volume fractions of continuous fiber filaments, the different kinds and the number of interfaces in 3D printed continuous fiber reinforced composites were displayed in table 1.

2.2.2. Specimen for peeling test

The specimens for the roller peeling test were selected according to the ASTM D3167 standard. As shown in Fig. 1 (c), the laminated specimens consisted of rigid and flexible parts. In the following denotation, PA-PA, C-C, K-K, C-PA and K-PA represented the different interfaces, and "PA" stood for PA matrix, "C" and "K" stood for continuous carbon fiber and continuous Kevlar fiber layers, respectively.

2.3. Characterization

The mechanical behaviors of printed composites were investigated by tensile testing using an MTS universal mechanical testing machine (E44, MTS Co., USA) with a 30 kN loading cell. Tensile tests were conducted at a cross-head speed of 10 mm/min and room temperature. The grip distance was set to 40 mm and the aligning of the longitudinal axis of the specimen with the grips was done. The extensometer (635.50F-25, MTS Co., USA) was used to capture the strain of the deformed specimens. Noted that the extensometer should be unloaded when reaching the maximum measure range (25 mm), due to the large strain plastic deformation of Kevlar fibers. The maximum stress was taken as the tensile strength. Note that each measurement was averaged from the results of five repeated and recorded tests.

The roller peel tests in the current study were performed to investigate the adhesion properties of the printed composites by the same mechanical testing machine with a 1 kN load cell. A cross-head loading rate of 100 mm/min was applied. The tests were performed at room temperature. A total of three specimens were tested for each test condition, and the average values were calculated with their standard deviation.

3. Results and discussion

3.1. Tensile behaviors

The tensile modulus, tensile strength and elongation at break of

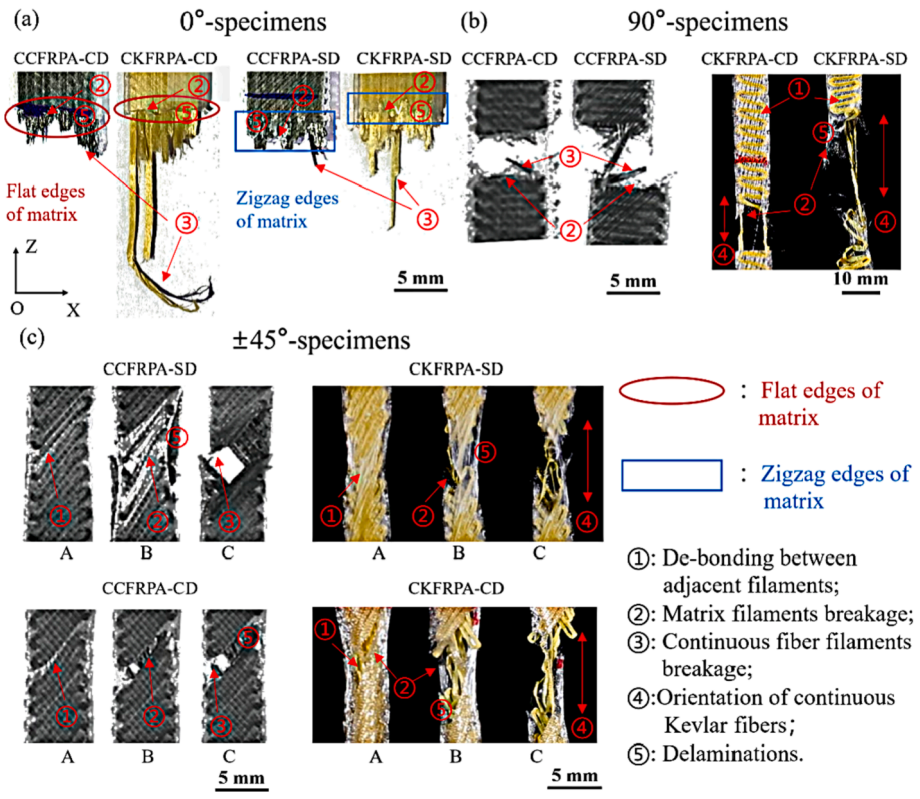

Fig. 3. Fractured sections for 3D printed (a) 0°, (b) 90° and (c) ± 45° continuous fiber reinforced composites along XOZ plane.

composites with different continuous fibers, fiber raster orientations and stacking sequences are presented in Fig. 2(a). Tensile stress–strain curves for all specimens are illustrated in Fig. 2(b–d). In Fig. 2, it can be seen that the tensile modulus and strengths of CCFRPA composites were all higher than those of CKFRPA composites, whatever fiber orientations and layer sequences. By contrast, the elongation at break of 0°-CCFRPA composites was closed to that of 0°-CKFRPA composites, and 90°-CCFRPA and ± 45°-CCFRPA presented lower elongation at break compared with 90°-CKFRPA and ± 45°-CKFRPA. Taking into account the stacking sequence, as shown in Fig. 2 (a), the tensile modulus and strength of 0° and ± 45° composites were sensitive to the stacking sequence. Meanwhile, the elongation at break of CD composites was closed to that of SD composites, except for 90°-CKFRPA.

To further understand the damage mode and failure mechanism of printed composites with different fiber reinforcements, stacking sequences and raster orientations, the images of samples stretched at different stages (A, B and C shown in Fig. 2) were captured. Note that only the ultimate failure (point C) images for 0° and 90° composites were exhibited. While the strain evolutions (A, B and C) for ± 45° composites were compared because they had different damage modes for two types of stacking sequences. In Fig. 3, generally, it can be seen that the main failure modes of printed composites included delamination, de-bonding between adjacent filaments, fibers and matrix breakage, near the localized rupture areas.

In Fig. 3(a), it could be observed that the major difference in the damage modes of 0° composites with two stacking sequences was the way of matrix breakage. Whatever the reinforced continuous fiber was, the composites with concentrated sequence showed a flat edge of matrix

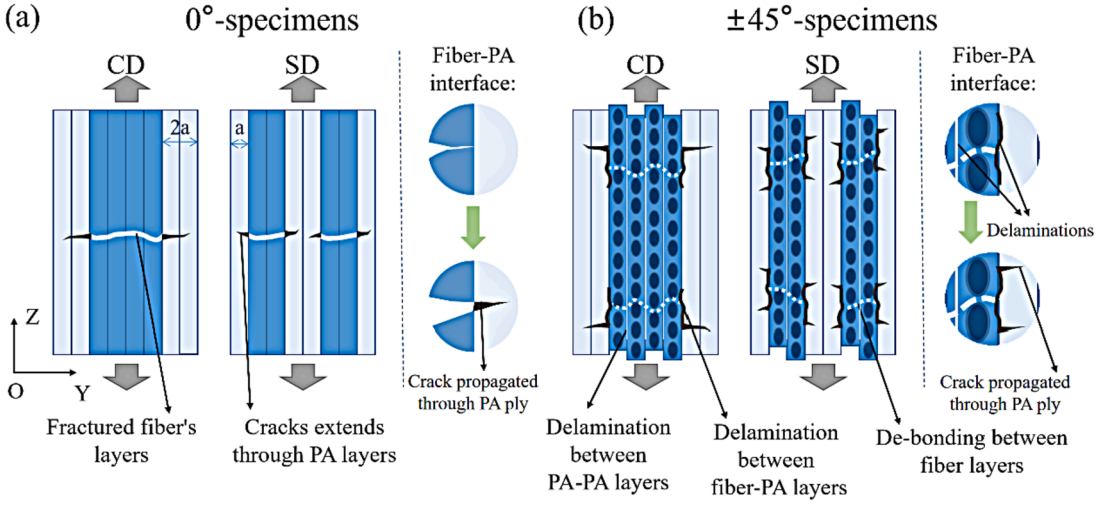

Fig. 4. Schematic presentation of damage mechanisms for 3D printed (a) 0° and (b) ± 45° continuous fiber reinforced composites along the YOZ plane.

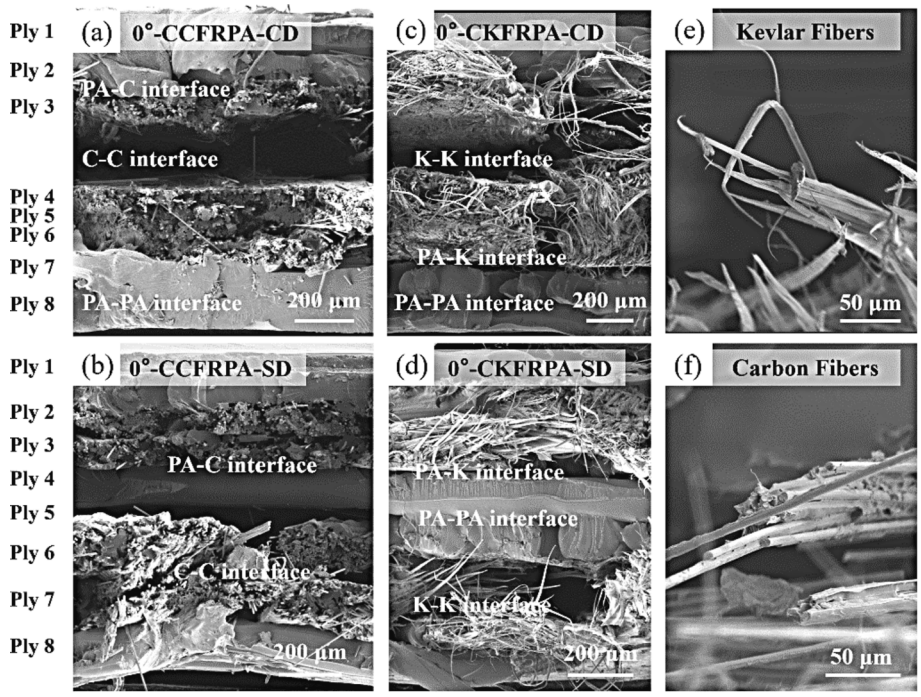

Fig. 5. The effect of stacking sequence on the fracture surface of the 3D printed 0° continuous fiber reinforced composites.

layer in the damage section, while composites with separated sequence exhibited a zigzag edge of the matrix. These phenomena perhaps could be attributed to the different numbers of matrix–matrix interfaces in CD and SD composites with 0° raster orientation. Specifically, 0° continuous fibers failed first as they had small breakage strain, causing out-of-plane normal cracks in the composite. PA matrix then continued to bear stress near the cracked zone, leading to stress concentration build-up in PA plies around the failed continuous fibers. As shown in Fig. 4(a), cracks in the PA plies initiated at two locations in CD composites as there were two fiber-PA interfaces and progressed through width. On contrary, in SD composites, cracks in the PA plies initiated at multiple locations as there were more fiber-PA interfaces However, cracks in SD composites propagated shorter than that in CD specimen before achieving the final breakage. These were perhaps the reason why 0°-CCFRCs-CD had slightly higher tensile strength and smoother breakage surface than 0°-CCFRCs-SD.

In Fig. 3(b), the damage modes of the 90° composites exhibited limited difference between the two stacking sequences, but showed significant between the two types of fiber reinforcement. In this figure, the fiber and matrix breakages of 90°-CCFRPA were easy to be observed, while the 90° continuous Kevlar fibers were oriented to the stretching direction without breakage in our study range, leading to a high tensile toughness [30]. Thus, the strength of the 90°-CCFRPA composite was perhaps mainly determined by the strength of the PA matrix and the lateral strength of the continuous carbon fiber, while the strength of the 90°-CKFRPA composite was probably dominated by the strength of the PA matrix. As the strength of matrix and lateral strength of continuous fibers were remarkable lower than the longitudinal strength of fibers,

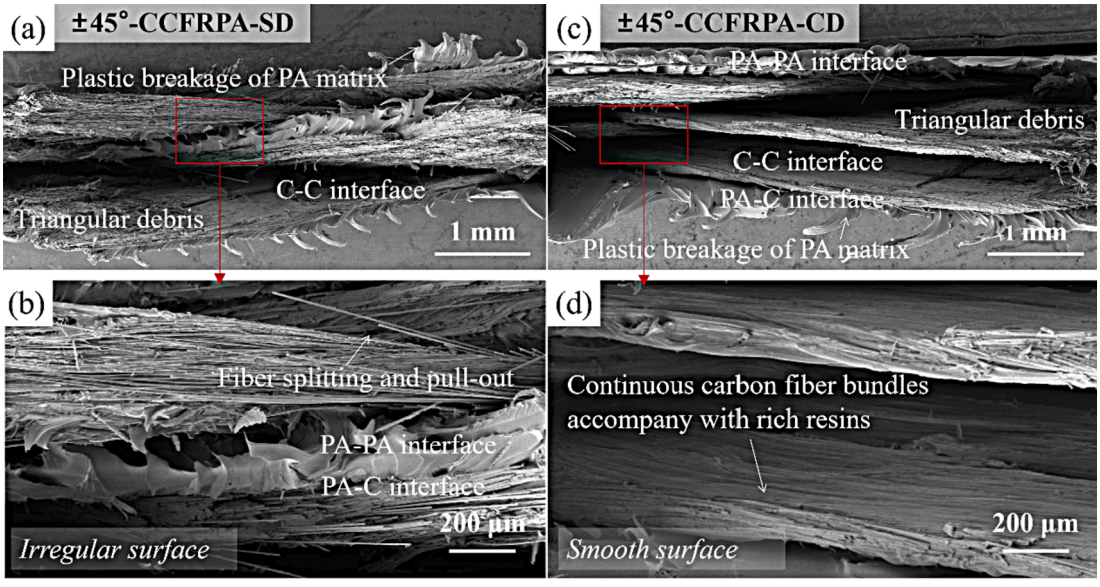

Fig. 6. SEM images of tensile fracture surface for the ± 45° composites with (a-b) SD and (c-d) CD stacking sequences.

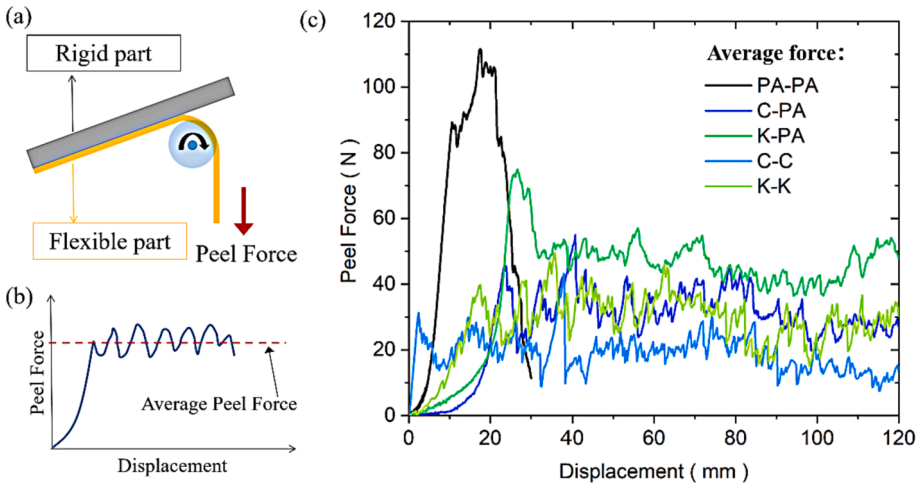

Fig. 7. Interfacial properties of 3D printed continuous fiber reinforced composites (a) illustration of peel tests, (b) the calculation method of average peel loads and (c) peel force–displacement curves.

the 90° composites owned the lowest tensile strength in the current study ranges. Meanwhile, the carbon fibers' lateral strength was higher compared to the strengths of matrix and Kevlar fibers, which could explain that the 90°-CCFRPA composite expressed a higher tensile strength than that of the 90°-CKFRPA composite.

Fig. 3(c) showed the damage evolution for ± 45° composites captured by a digital camera at points A, B, and C marked in Fig. 2(d). In this figure, point A corresponded to the initial damage stage, while points B and C represented the damage evolution stages, respectively. In the initial damage stage, the de-bonding (white lines in images) between adjacent continuous fiber filaments was discovered in all ± 45° composites, whatever the staking sequences and reinforcements (Fig. 3(c) and Fig. 4(b)). The continuous fiber filaments were observed to de-bond first, perhaps because they have weaker interfacial bonding than the PA matrix [12]. In the damage propagation stage at point B, the PA matrix breakages and delamination were found in all the composites. A slight degree of matrix filaments breakages was discovered in SD composites, while CD composites showed serious filaments breakages in the matrix. This phenomenon was probably suggested that the separated sequence of continuous fiber in composites retarded the de-bonding and cracks propagation through the whole specimen, further delaying the delamination between fiber-PA interfaces and microcracking initiation in PA plies, which resulted in a higher tensile strength of SD specimens compared to CD specimens. Herakovich et al. [31,32] reported similar results that in carbon/epoxy ± 45° angle ply laminates, the "separated" stacking sequence of the laminates produced a single diagonal failure path with fiber fractures. Whereas the "concentrated" stack failed predominantly by delamination and limited fiber fractures at a lower strength, which attributed to the higher interlaminar shear stresses. Finally, at point C, the continuous fiber filaments breakages were observed in ± 45°-CCFRPA but not in ± 45°-CKFRPA, and the Kevlar fibers were orientated along the tensile direction. This phenomenon resulted in the lower tensile strength but higher elongation at break of ± 45°-CKFRPA compared to ± 45°-CCFRPA composite. In order to prove the influence of interfaces induced by stacking sequence on the deformation properties of the composites, we further investigated the fractured surfaces of 0° and ± 45° specimens by using SEM (Fig. 5 and Fig. 6). The mechanical behaviors of 90° samples were found to be less sensitive to the stacking sequence (Fig. 2), the microscopic features of 90° samples, therefore, were not discussed.

Fig. 5 shows the fracture surfaces of 0° composites after tensile testing. In this figure, it can be seen that the printed composites had different kinds and numbers of interfaces between printed plies depending on the designed stacking sequence. As shown in Fig. 5 (a-d), PA plies in the composites were tightly affixed together without visible delamination. However, delamination was easily observed between the C–C and K-K interfaces. In comparison, it seemed that C-PA and K-PA interfaces had fewer de-bonding problems than those of the C–C and K-K interfaces. These observed microscopic features could be used to explain that the composites with concentrated continuous fiber layer distribution owned more PA-PA interfaces with better interfacial adhesion, resulting in a slightly higher tensile strength than the SD composite. In addition, the ductile fractured continuous Kevlar fibers (Fig. 5 (e)) proved the toughening effects of Kevlar fibers. The limited deformation behaviors of the 0° CCFRPA composite could be explained by the brittle carbon fibers (Fig. 5 (f)), which demonstrated smooth fractured surfaces with invisible plastic deformation.

On the contrary, ±45°-SD specimens presented higher tensile strength than ± 45°-CD ones. As shown in Fig. 6, for ± 45°-CCFRPA specimens, irregular surfaces of continuous fiber bundles in SD composites could be found, while the continuous fiber bundles in CD composites showed smoother surfaces. Specifically, a large number of continuous carbon fibers in ± 45°-CCFRPA-SD were pulled out and broke along ± 45° directions compared to 45°-CCFRPA-CD (Fig. 6). Tensile strength of ± 45°-CCFRPA-SD was therefore slightly higher than that of ± 45°-CCFRPA-CD. In addition, the visible delamination in ± 45° composites was observed between carbon fiber plies, while the less debonding problem was found for other interfaces, which were following the phenomenon in 0° composites. To further understand the contribution of interfaces, the next section would focus on the quantification of interfacial strength.

3.2. *Interfacial strength*

The adhesion properties of interfaces in printed composites were evaluated using floating roller peeling tests. Fig. 7 shows the representative peel force–displacement curves for various laminated composites in peeling tests. Note that the continuous fibers for the peeling test specimen were printed by 0° raster orientation. The ± 45° peeling specimens showed similar results to the 0° one [33]. And the specimens with 90° continuous fibers were hard to peel.

In Fig. 7, the peel forces for all composites fluctuated steadily after the initial rising. However, the forces for the PA-PA interface dropped suddenly after 20 mm displacement. The average peel loads were determined along 100 mm peeling lengths ranging from 20 mm to 120 mm, discarding the first 20 mm displacement (except for the PA-PA interface) [34,35]. According to this method, as seen in Fig. 7 (c), the average peel loads for the PA-PA were higher than that of C–C, followed by the K-K, C-PA and K-PA. This tendency was in accord with our observation in Figs. 3-6.

Table 1
Filament volume fraction, interface type and number of 3D printed continuous fiber reinforced composites.

Specimens	Filament volume fractionin specimens (vol. %)			Fiber-fiber layer interfaces' number		Fiber-matrix layer interfaces' number		Matrix-matrix layer interfaces' number
	Matrix (PA)	Carbon fibers (C)	KevlarFibers (K)	C–C	K-K	C-PA	K-PA	PA-PA
0°-CCFRPA-CD	58.3	41.7	0	3	0	2	0	2
0°-CCFRPA-SD				2	0	4	0	1
0°-CKFRPA-CD	62.7	0	37.3	0	3	0	2	2
0°-CKFRPA-SD				0	2	0	4	1
90°-CCFRPA-CD	61.1	38.9	0	3	0	2	0	2
90°-CCFRPA-SD				2	0	4	0	1
90°-CKFRPA-CD	64.7	0	35.3	0	3	0	2	2
90°-CKFRPA-SD				0	2	0	4	1
±45°-CCFRPA-CD	62.2	37.8	0	3	0	2	0	2
±45°-CCFRPA-SD				2	0	4	0	1
±45°-CKFRPA-CD	66.7	0	33.3	0	3	0	2	2
±45°-CKFRPA-SD				0	2	0	4	1

Table 2
The interface strength coefficient..$a^*(x)$

Interfaces	Average peeling force (N)	$a^*(x)$
PA-PA	100.70	1.00
C-PA	31.02	0.31
K-PA	47.10	0.47
C–C	18.67	0.19
K-K	30.35	0.30

Table 3
Adopted elastic properties of each component for the printed materials [21].

Material Properties	Carbon	Kevlar	PA
Longitudinal elastic modulus E_1 (MPa)	85,000	30,000	380
Transverse elastic modulus E_2 (MPa)	26,000	10,000	380
In-plane shear modulus G_{12} and G_{23} (MPa)	5000	5000	141
Poisson's ratio ν_{12}	0.3	0.2	0.35

4. Modelling

As discussed above, the interfaces played a non-ignorable role in the tensile behavior of printed composites with continuous fibers. Different from the composites manufactured by traditional methods, fiber filled composites prepared by the FDM method showed weak initial bonding between layers and layers, due to the less printing pressure during the printing process. We therefore in this work introduced the interfacial strength ratio as a coefficient into the volume average stiffness model, to take into account the contribution of the interface to the mechanical properties of 3D printed composites [36,37]. Here, the PA-PA interface's peeling force (F_{PA-PA}) was used as a correlative value, and the ratios of other interfaces' peeling force (F_x) to that of F_{PA-PA} were used as strengthening coefficient, $a^*(x)$, estimating from the following equation (x represented the matrix (m) or fibers (f)) and the values were listed in Table 2:

$$a^*(x) = F_x / F_{(PA-PA)} (x = PA-PA, C-C, K-K, C-PA \text{ and } K-PA) \quad (1)$$

Then this strengthening coefficient, $a^*(x)$, was incorporated into the volume average stiffness approach to compute the stiffness Q of the composites, based on the stiffness of matrix and continuous fiber as follows:

$$\begin{cases} Q = Q_m{}' + Q_f{}' \\ Q_m{}' = \sum_{i=1}^{n} a^*{}_x V_{mi} \overline{Q}_m (n = the number of matrix plies) \\ Q_f{}' = \sum_{j=1}^{n} a^*{}_x V_{fj} \overline{Q}_f (n = the number of fiber plies) \end{cases} \quad (2)$$

where the V_{mi} and V_{fj} respectively meant the volume fractions of each matrix (PA) layer and continuous fiber layer, details of volume fractions for continuous fiber and matrix in the composites were given in Table 1. $\overline{Q}_m$ and $\overline{Q}_f$ were respectively the stiffness of matrix and fibers in the global coordinate system, which were related to Q_m and Q_f in the fiber coordinate systems as:

$$\overline{Q}_m = [T]^T Q_m [T] \quad (3)$$

$$\overline{Q}_f = [T]^T Q_f [T] \quad (4)$$

here, the stiffness of the matrix Q_m, the stiffness of fibers Q_f and transformation matrix [T] was defined as follows [21]:

$$Q_m = \begin{bmatrix} \frac{E}{1-\nu^2} & \frac{\nu E}{1-\nu^2} & 0 \\ \frac{\nu E}{1-\nu^2} & \frac{E}{1-\nu^2} & 0 \\ 0 & 0 & G \end{bmatrix} \quad (5)$$

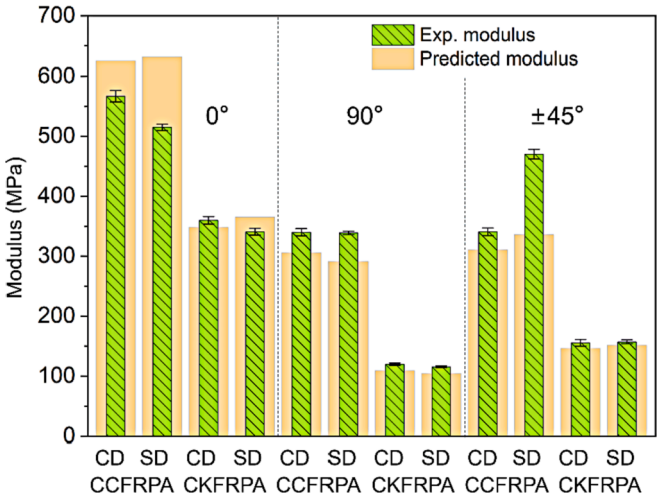

Fig. 8. Comparison of experimentally measured and predicted elastic modulus.

$$Q_f = \begin{bmatrix} \frac{E_1}{1-\nu_{12}\nu_{21}} & \frac{\nu_{12}E_2}{1-\nu_{12}\nu_{21}} & 0 \\ \frac{\nu_{12}E_2}{1-\nu_{12}\nu_{21}} & \frac{E_2}{1-\nu_{12}\nu_{21}} & 0 \\ 0 & 0 & G_{12} \end{bmatrix} \tag{6}$$

$$[T] = \begin{bmatrix} cos^2\theta & sin^2\theta & sin\theta cos\theta \\ sin^2\theta & cos^2\theta & -sin\theta cos\theta \\ sin\theta cos\theta & -sin\theta cos\theta & cos^2\theta - sin^2\theta \end{bmatrix} \tag{7}$$

in this, θ was the angle of matrix and fibers;E, G and ν were respectively the elastic modulus, shear modulus and Poisson's ratio of the matrix; and E_1, E_2, G_{12}, ν_{12} were respectively the elastic modulus, shear modulus and Poisson's ratio of fibers, and the values were given in Table 3:

The elastic modulus, E_{11}, of the composites can be obtained from the components of the compliance matrix [S] as:

$$E_{11} = \frac{1}{S_{11}} \tag{8}$$

where S_{11} was the components of the compliance matrix [S], which was the inversion of the stiffness matrix [Q] given in Eq. (2).

Fig. 8 displays comparison results of the elastic modulus obtained from experimental data and the proposed model considering interface contribution. In this figure, it can be seen that our proposed model could well estimate the elastic modulus for CKFRPA composites with different staking sequences and fiber orientations, by showing small gaps between the experimental and computed results. In contrast, the differences in the elastic modulus for CCFRPA were slightly larger.

5. Conclusions

In this paper, we studied the tensile behaviors of 3D printed continuous fiber filled composites with different reinforcement fibers, stacking sequences and raster orientations. The structural evolutions and failure features of the composites induced by strain were analyzed by digital camera and scanning electron microscopy (SEM), in order to reveal the deformation and failure mechanisms of composites with the consideration of interfaces. It was found that the tensile strength for 0°-CD composites was higher than that of 0°-SD ones because the CD composites owned better adhesion interfaces. Nevertheless, ±45°-SD specimens presented higher tensile strength compared with ± 45°-CD ones, attributed to the separated staking sequence of continuous fiber in composites, delaying the delamination and microcracking initiation in plies. Thus, the designed interfaces between different material layers played an important role in the mechanical properties of printed composites. The interfacial strength between different materials was quantified by a roller peeling test. The average peel loads for the PA-PA interface were higher than that of others. An analytical approach was introduced to predict the stiffness behavior of the printed composites by introducing an interfacial strengthening coefficient into the volume average stiffness model. The predictions of stiffness, for the 3D printed continuous fiber filled composites with different fibers, stacking sequences and raster orientations, were in good agreement with experimental results.

In the current study, the interfacial strengthening coefficient was assumed to evenly contribute to adjacent printed layers. However, as the material contribution to the interface was different, the interface closed to different materials should have different properties. Therefore, the unequal contribution of the interface to different ply needed to be investigated in the next study.

CRediT authorship contribution statement

Shixian Li: Data curation, Methodology, Writing – original draft. **Kui Wang:** Conceptualization, Writing – review & editing. **Wanying Zhu:** Software. **Yong Peng:** Resources. **Said Ahzi:** Conceptualization. **Francisco Chinesta:** Writing – review & editing.

Declaration of Competing Interest

The authors declare that they have no known competing financial interests or personal relationships that could have appeared to influence the work reported in this paper.

Acknowledgements

This work was supported by the National Natural Science Foundation of China (No. 51905555), the Hu-Xiang Youth Talent Program (No. 2018RS3002 and 2020RC3009), the Innovation-Driven Project of Central South University (No. 2019CX017).

References

[1] S.F. Kabir, K. Mathur, A.-F.-M. Seyam, A critical review on 3D printed continuous fiber-reinforced composites: History, mechanism, materials and properties, Compos. Struct. 232 (2020), 111476.
[2] X. Wang, M. Jiang, Z. Zhou, J. Gou, D. Hui, 3D printing of polymer matrix composites: A review and prospective, Compos. B Eng. 110 (2017) 442–458.
[3] U.M. Dilberoglu, B. Gharehpapagh, U. Yaman, M. Dolen, The role of additive manufacturing in the era of industry 4.0, Procedia Manuf. 11 (2017) 545–554.
[4] M. Rinaldi, T. Ghidini, F. Cecchini, A. Brandao, F. Nanni, Additive layer manufacturing of poly (ether ether ketone) via FDM, Compos. B Eng. 145 (2018) 162–172.
[5] G. Ma, Z. Li, L. Wang, F. Wang, J. Sanjayan, Mechanical anisotropy of aligned fiber reinforced composite for extrusion-based 3D printing, Constr. Build. Mater. 202 (2019) 770–783.
[6] C.E. Corcione, E. Palumbo, A. Masciullo, F. Montagna, M.C. Torricelli, Fused Deposition Modeling (FDM): An innovative technique aimed at reusing Lecce stone waste for industrial design and building applications, Constr. Build. Mater. 158 (2018) 276–284.
[7] K. Wang, R. Cai, Z. Zhang, J. Liu, S. Ahzi, Y. Peng, Y. Rao, Compressive behaviors of 3D printed polypropylene-based composites at low and high strain rates, Polym. Test. 103 (2021), 107321.
[8] F. Wang, J. Wu, L. Hu, C. Yu, B. Wang, X. Huang, K. Miller, A. Wittek, Evaluation of the head protection effectiveness of cyclist helmets using full-scale computational biomechanics modelling of cycling accidents, J. Saf. Res. 80 (2022) 109–134.
[9] M. Dawoud, I. Taha, S.J. Ebeid, Mechanical behaviour of ABS: An experimental study using FDM and injection moulding techniques, J. Manuf. Processes 21 (2016) 39–45.
[10] F. Van Der Klift, Y. Koga, A. Todoroki, M. Ueda, Y. Hirano, R. Matsuzaki, 3D printing of continuous carbon fibre reinforced thermo-plastic (CFRTP) tensile test specimens, Open J. Compos. Mater. 6 (1) (2016) 18–27.
[11] M. Heidari-Rarani, M. Rafiee-Afarani, A. Zahedi, Mechanical characterization of FDM 3D printing of continuous carbon fiber reinforced PLA composites, Compos. B Eng. 175 (2019), 107147.
[12] A.N. Dickson, J.N. Barry, K.A. McDonnell, D.P. Dowling, Fabrication of continuous carbon, glass and Kevlar fibre reinforced polymer composites using additive manufacturing, Addit. Manuf. 16 (2017) 146–152.
[13] H. Brooks, C. Wright, Title: 3D printing of continuous Kevlar fibre reinforced composites, 2019.
[14] Y. Peng, Y. Wu, K. Wang, G. Gao, S. Ahzi, Synergistic reinforcement of polyamide-based composites by combination of short and continuous carbon fibers via fused filament fabrication, Compos. Struct. 207 (2019) 232–239.
[15] Y. Peng, Y. Wu, S. Li, K. Wang, S. Yao, Z. Liu, H. Garmestani, Tailorable rigidity and energy-absorption capability of 3D printed continuous carbon fiber reinforced polyamide composites, Compos. Sci. Technol. 199 (2020) 108337.
[16] D. Yavas, Z. Zhang, Q. Liu, D. Wu, Interlaminar shear behavior of continuous and short carbon fiber reinforced polymer composites fabricated by additive manufacturing, Compos. B Eng. 204 (2021), 108460.
[17] J.G. Díaz-Rodríguez, A.D. Pertúz-Comas, O.A. González-Estrada, Mechanical properties for long fibre reinforced fused deposition manufactured composites, Composites Part B: Engineering (2021) 108657.
[18] H. Dou, Y. Cheng, W. Ye, D. Zhang, J. Li, Z. Miao, S. Rudykh, Effect of process parameters on tensile mechanical properties of 3D printing continuous carbon fiber-reinforced PLA composites, Materials 13 (17) (2020) 3850.
[19] Y. Ming, S. Zhang, W. Han, B. Wang, Y. Duan, H. Xiao, Xiao, Investigation on process parameters of 3D printed continuous carbon fiber-reinforced thermosetting epoxy composites, Addit. Manuf. 33 (2020), 101184.
[20] P.K. Mishra, P. Senthil, Prediction of in-plane stiffness of multi-material 3D printed laminate parts fabricated by FDM process using CLT and its mechanical behaviour under tensile load, Mater. Today Commun. 23 (2020), 100955.
[21] H. Al Abadi, H.-T. Thai, V. Paton-Cole, V. Patel, Elastic properties of 3D printed fibre-reinforced structures, Compos. Struct. 193 (2018) 8–18.
[22] G.W. Melenka, B.K. Cheung, J.S. Schofield, M.R. Dawson, J.P. Carey, Evaluation and prediction of the tensile properties of continuous fiber-reinforced 3D printed structures, Compos. Struct. 153 (2016) 866–875.

[23] S.A. Tofail, E.P. Koumoulos, A. Bandyopadhyay, S. Bose, L. O'Donoghue, C. Charitidis, Additive manufacturing: Scientific and technological challenges, market uptake and opportunities, Mater. Today 21 (1) (2018) 22–37.
[24] P. Cheng, K. Wang, X. Chen, J. Wang, Y. Peng, S. Ahzi, C. Chen, Interfacial and mechanical properties of continuous ramie fiber reinforced biocomposites fabricated by in-situ impregnated 3D printing, Ind. Crops Prod. 170 (2021), 113760.
[25] Z. Hou, X. Tian, Z. Zheng, J. Zhang, L. Zhe, D. Li, A.V. Malakhov, A.N. Polilov, A constitutive model for 3D printed continuous fiber reinforced composite structures with variable fiber content, Compos. B Eng. 189 (2020), 107893.
[26] T. Liu, X. Tian, M. Zhang, D. Abliz, D. Li, G. Ziegmann, Interfacial performance and fracture patterns of 3D printed continuous carbon fiber with sizing reinforced PA6 composites, Compos. A Appl. Sci. Manuf. 114 (2018) 368–376.
[27] Y. Wu, K. Wang, V. Neto, Y. Peng, R. Valente, S. Ahzi, Interfacial behaviors of continuous carbon fiber reinforced polymers manufactured by fused filament fabrication: A review and prospect, Int. J. Mater. Form. 15 (3) (2022) 1–18.
[28] J.M. Chacón, M.A. Caminero, P.J. Núñez, E. García-Plaza, I. García-Moreno, J. M. Reverte, Additive manufacturing of continuous fibre reinforced thermoplastic composites using fused deposition modelling: Effect of process parameters on mechanical properties, Compos. Sci. Technol. 181 (2019) 107688.
[29] K. Wang, S. Li, Y. Wu, Y. Rao, Y. Peng, Simultaneous reinforcement of both rigidity and energy absorption of polyamide-based composites with hybrid continuous fibers by 3D printing, Compos. Struct. 267 (2021), 113854.
[30] S. Iqbal, R. Khan, Effect of brushing & abrading of laminae on the mode I fracture toughness of glass fiber/epoxy composite, Constr. Build. Mater. 261 (2020), 120508.
[31] C.T. Herakovich, Influence of layer thickness on the strength of angle-ply laminates, J. Compos. Mater. 16 (3) (1982) 216–227.
[32] C.T. Herakovich, R.D. Schroedter III, A. Gasser, L. Guitard, Damage evolution in [±45] s laminates with fiber rotation, Compos. Sci. Technol. 60 (15) (2000) 2781–2789.
[33] S. Solaimurugan, R. Velmurugan, Influence of in-plane fibre orientation on mode I interlaminar fracture toughness of stitched glass/polyester composites, Compos. Sci. Technol. 68 (7–8) (2008) 1742–1752.
[34] M.M. Arouche, S. Budhe, M.D. Banea, S. Teixeira de Freitas, S. de Barros, Interlaminar adhesion assessment of carbon-epoxy laminates under salt water ageing using peel tests, Proc. Inst. Mech. Eng., Part L: J. Mater.: Des. Appl. 233 (8) (2019) 1555–1563.
[35] A. Kubit, T. Trzepieciński, B. Krasowski, J. Slota, E. Spišák, Strength analysis of a rib-stiffened GLARE-based thin-walled structure, Materials 13 (13) (2020) 2929.
[36] H. Whitworth, A stiffness degradation model for composite laminates under fatigue loading, Compos. Struct. 40 (2) (1997) 95–101.
[37] R.C. Cammarata, K. Sieradzki, Effects of surface stress on the elastic moduli of thin films and superlattices, Phys. Rev. Lett. 62 (17) (1989) 2005–2008.
[38] Pascual-González C, Iragi M, Fernández A, Fernández-Blázquez J, Aretxabaleta L, Lopes C, An approach to analyse the factors behind the micromechanical response of 3D-printed composites, Compos. B Eng. 186 (2020), 107820.